Materials Today Sustainability 32 (2025) 101222

Contents lists available at ScienceDirect

Materials Today Sustainability

journal homepage: www.journals.elsevier.com/materials-today-sustainability

Thermal enhancement of phase change materials using nanoparticles and novel finned structures

Hassan Waqas [a], Meraj Ali Khan [b], Mohib Hussain [c], Zunhua Zhang [a,*]

[a] School of Naval Architecture, Ocean and Energy Power Engineering, Wuhan University of Technology, Wuhan, Hubei, 430063, China
[b] Department of Mathematics and Statistics, College of Science, Imam Mohammad Ibn Saud Islamic University (IMSIU), Riyadh, 11566, Saudi Arabia
[c] School of Mathematics and Statistics, Northwestern Polytechnical University, Xian, 710072, China

ARTICLE INFO

Keywords:
Melting process
Heat transfer
Fin
Fe_3O_4 - Cunanoparticles
Molten salt PCM
Artificial neural network

ABSTRACT

Phase change materials (PCMs) have proven vital in thermal energy storage systems due to their remarkable energy density and capacity to sustain a stable temperature. This study examines how adding new dendritic fin structures positioned in the lower region can improve heat transfer and melting kinetics in a molten salt-based nano-enhanced phase change material (NEPCM) with Fe_3O_4 - *Cu* hybrid nanoparticles inside rectangular enclosures. A baseline example without fins, a second case with dendritic fins whose branch lengths decrease toward the bottom (type 1), and a third case with dendritic fins whose branch lengths increase toward the bottom (type 2) are the three different configurations that are examined in this study. The thermal behavior was numerically modelled using the porosity-enthalpy method. We also developed an artificial neural network (ANN) model with a multilayer perceptron architecture that includes two hidden layers to predict melting characteristics and thermal performance parameters, training it on both computational and experimental datasets. When paired with hybrid nanoparticles, total melting was accomplished about 41 % faster. With correlation coefficients above 0.98 and mean relative error below 3.5 % under all test settings, the created ANN model was able to predict melting percent, average temperature, and Nusselt number. The ANN model's sensitivity analysis revealed that the two most important factors influencing thermal performance were the concentration of nanoparticles and the fin branch length ratio. For future studies, it would be beneficial to focus on optimizing the parameters of these dendritic fin structures and to investigate the ideal Fe_3O_4 - *Cu* ratios to achieve maximum thermal performance while ensuring colloidal stability.

1. Introduction

Thermal energy storage (TES) has emerged as a key technology for resolving the intermittency issues with renewable energy sources as a result of the global push to move toward sustainable energy systems. Rapid decarbonization across all sectors is required to meet climate targets set by international accords, and energy storage is becoming the link between inconsistent demand patterns and variable generation. High energy density, isothermal operation during phase transition, and temperature range adaptability are three particularly attractive benefits of latent heat thermal energy storage using phase change materials (PCMs) among the range of TES technologies. Phase change materials (PCMs) are incredibly valuable for various applications, such as concentrated solar power plants, industrial waste heat recovery, and thermal management in buildings. Recent advancements in phase change material (PCM) production have beyond conventional melt-mixing and impregnation techniques, including methods such as 3-D printing, electrospinning, and sol-gel templating. These novel techniques enable meticulous regulation of pore structure and overall morphology. These novel technologies not only accelerate manufacturing but also permit the incorporation of conductive or developing chemicals into the scaffold during fabrication as required. A comprehensive comparison of these approaches is now unfeasible; nonetheless, their rapid proliferation indicates an increasing array of instruments for the development of future-oriented PCM. However, despite their potential, traditional PCMs have some key limitations that hinder their widespread use. A significant problem is the low thermal conductivity of applied PCMs, particularly those that are salt-based, which slows down heat transfer during both charging and discharging cycles. At comparison to their bulk equivalents, phase change materials

* Corresponding author. School of Naval Architecture, Ocean and Energy Power Engineering, Wuhan University of Technology, Wuhan, Hubei, 430063, China.
E-mail address: zunhuazhang@whut.edu.cn (Z. Zhang).

https://doi.org/10.1016/j.mtsust.2025.101222
Received 7 June 2025; Received in revised form 26 July 2025; Accepted 13 September 2025
Available online 15 September 2025
2589-2347/© 2025 The Author(s). Published by Elsevier Ltd. This is an open access article under the CC BY-NC license (http://creativecommons.org/licenses/by-nc/4.0/).

(PCMs) at micro- or nanoscale demonstrate much greater contact areas. Moreover, encapsulation is crucial for safeguarding the extensive surface region of nano or micro PCMs from sintering Hawlader et al. [1]. Additionally, the surface modification of micro/nano-sized PCMs is readily attainable, allowing for their dispersion in a heat transfer fluid (HTF), hence augmenting the application capacity of PCMs Aftab et al. [2]. Although PCMs are appropriate for several thermal applications, the actual implementation of solid–liquid PCMs remains constrained by various challenges. Liquid PCMs may leak during the TES process, hence diminishing their TES capacity and cycle stability. Specifically, the use of acids and molten salts as PCMs may lead to corrosion of critical components inside devices or facilities, hence diminishing their operational lifespan and potentially resulting in safety hazards. A potential resolution to these problems is the encapsulation of PCMs at the micro- or nano-scale Shchukina et al. [3]. Encapsulated PCMs are referred to as micro-encapsulated PCMs or nano encapsulated PCMs, based on the size they have. By purposefully including nanoscale particles into the PCM matrix, nano-enhanced phase change materials (NEPCMs) offer a smart solution to different constraints of simple PCMs like low thermal conductivity and limited surface area. The effective thermal conductivity, specific heat capacity, and phase change kinetics of the composite material can all be significantly changed by adding nanoparticles with better thermal characteristics. Colak [4] worked on Numerical investigation with deep learning for thermal energy storage unit utilizing the nano particles with in the complex enclosure such as wavy shape. Thirumalaivasan et al., [5], well-chosen nanoparticles can influence nucleation behavior and interfacial heat transfer mechanisms while also increasing thermal conductivity by 20–45 % at remarkably low volume fractions (0.5–2 %). The way nanoparticles interact with PCM gives rise to a variety of complex phenomena at the micro and nanoscale. This includes Brownian motion, the creation of interfacial layers, and the establishment of percolation networks, all of which contribute to changes in thermal behavior. Iron oxide Fe_3O_4 and copper (Cu) have become particularly attractive options for NEPCM formulation among the wide range of possible nano additives. Copper nanoparticles offer exceptionally high intrinsic thermal conductivity (398 W/m·K), which can create efficient thermal conduction pathways within the PCM matrix Benyahia et al., [6], while Fe_3O_4 nanoparticles have special magnetic properties that promote enhanced dispersion stability and the possibility of magnetically-assisted heat transfer Ho and Pan, [7]. These nanoparticles have the potential to have synergistic effects that are greater than those of either element alone when they are carefully mixed to create hybrid form. Due to complimentary surface contacts and altered electro kinetic properties, hybrid nano PCM systems showed improved thermal performance and greater colloidal stability when compared to mono-PCM systems Kibria et al., [8]. Abdolahimoghadam and Rahimi., [9], presented an experimental-designed for thermal energy storage (TES) system to examine the capacity of hybrid nano PCM. They employed Graphene-Copper hybrid nanoparticles for investigation. Molten salts are an excellent base material for high-temperature thermal storage, usually functioning within a range of 200-600 °C, depending on their specific composition. We selected them for this research due to their thermal stability, relatively high volumetric heat capacity, and their established compatibility with concentrated solar power and industrial systems. Common formulations consist of binary and ternary mixtures of nitrates, chlorides, and carbonates, each with its own unique thermal properties and melting points (Kenisarin, [10]. Yu et al., [11], investigated the melting process of a high-temperature molten salt in a container. The findings indicated that natural convection caused nonlinear displacement of the interface between the phases and segregation in the temperature of the fluid component. Yang et al., [12] examined the heat sensing capacity technique to assess the thermal storage efficiency of a molten salt-based horizontal TES apparatus. The influence of deviation, heat transfer liquid temperature, fin quantity, and fin size on the thermal storage efficacy of the TES system was examined. Although previous studies have explored various nanoparticle enhancements in molten salt PCMs, like TiO_2 and Al_2O_3 Khalid et al., [13], SiO_2 Lasfargues et al., [14], and Al_2O_3 Hussain et al., [15], there's still a significant lack of systematic investigation into Fe_3O_4 - Cu hybrid systems in the literature. Geometric engineering using expanded surfaces is an additional tactic for improving thermal performance in addition to material modification. Additional heat transfer channels offered by finned structures integrated into PCM containment systems can significantly speed up the melting and solidification processes. Several factors, including as material, spacing, direction, thickness, and geometric configuration, affect how effective fins are. While Andreozzi et al., [16] showed that quantitative extent to improve the heat transfer mechanism to improve their thermal performance of the heat exchangers, Kalapala and Devanuri [17] showed that well-designed longitudinal fins could cut total melting time by up to 60 % when compared to no fins systems. The contact area between the phase change material (PCM) and the heat transfer surface is increased by the fin-driven augmentation. In addition to providing the best possible conduction channels, this design deftly breaks the liquid-solid barrier during the phase change. Over the past ten years, there has been a significant evolution in the literature regarding PCM thermal enhancement. The impacts of nanoparticles on phase change processes were first studied by Khodadadi and Hosseinizadeh [18], and other studies examined particle-PCM interactions that were more intricate. Copper nanoparticles in paraffin were studied by Ranjbar et al., [19], who observed that at greater loadings, conductivity increased and latent heat decreased. Bondarev et al., [20] worked on thermal energy storage using nano additives phase change materials using a numerical simulation of conjugate thermal convection partially filled with metal foam. Rong et al., [21] worked on experimental and theoretical investigation of molten salt using innovative composite of nano fluid for the conversion and storage of solar energy photothermal. Trigui et al., [22] worked to improve the thermal conductivity of organic PCM using copper microparticles. In particular, for molten salt systems, Muñoz-Sánchez et al., [23]looked into silica nanoparticles in solar salt, while Wu et al., [24] examined various ceramic nanoparticles in chloride eutectics. Both studies pointed out the complex relationships between thermal performance, how well the particles disperse, and the number of particles used. Research on finned geometries has advanced significantly from simple rectangular forms to complex, optimized designs. Sardari et al., [25] employed topology optimization in their computer studies to find several unexpected fin configurations that significantly increased melting rates. In the meantime, Y-shaped fins were examined in further detail by Khedher et al., [26], who found that they enhanced conduction and maintained those beneficial natural convection currents. Wang et al., [27] tested these numerical calculations and discovered that proper fin placement might reduce melting time by 52 % while utilizing 30 % less fin material than conventional designs. Qasem et al., [28] investigated the impact of tree-shaped fins to boost the thermal energy storage. They establish that the combination of elongated sub-fins with PCM component leads to an increment in the heat transfer dispersal, ensuing in a 75.7 % decrease in melting time. Li et al., [29] studied hub-shaped fin for thermal performance improvement in a shell-tube thermal energy storage system. Their findings indicate that the fin architecture having a sub-branch inclination of 45° possesses the maximum melting percentage, resulting in a 34.2 % amplification of the procedure of melting. Despite these developments, there are still a lot of unanswered questions about the combined use of hybrid nanoparticles and fin geometry optimization in molten salt PCMs. Although individual enhancement tactics have been studied, little is known about their combined effects, including possible interaction mechanisms, ideal concentration ratios, and geometric arrangements. This research deficiency is particularly obvious for the Fe_3O_4 - Cu hybrid system in molten salt matrices, where the interplay between magnetic characteristics, metallic conduction, and extended surfaces has not been thoroughly studied. In this study, we dive deep into the thermal behavior and melting properties of a molten salt-based phase change material

(PCM) enhanced with Fe_3O_4 - Cu hybrid nanoparticles, all while utilizing optimized fin designs. By merging computational fluid dynamics modeling, we explore the fundamental heat transport mechanisms, phase change kinetics, and thermal performance metrics of this cutting-edge composite system. We carefully evaluate how different operating conditions, fin shapes, and nanoparticle concentration ratios influence the melting rate, temperature distribution, and overall thermal efficiency. By demonstrating the benefits of simultaneously employing material and geometric advancements, this work represents a significant advancement in thermal energy storage technology. Fe_3O_4 and - Cu nanoparticles are combined to form a unique hybrid system that enhances thermal transport by utilizing both magnetic and metallic conductivity. Furthermore, bigger heat transfer channels are provided by the astute use of fins, which complement the nanoscale adjustments. This combination of enhancement techniques at various scales addresses the fundamental thermal issues that conventional phase change materials (PCMs) encounter and lays the groundwork for novel design concepts in high-performance latent heat storage systems, especially in industrial and renewable energy context

2. Mathematical simulation:

We have a phase change material (PCM) called molten salt inside a rectangular-finned in square cavity (see Fig. 1). PCM rectangular enclosure with 30 mm length and 25 mm height. The radius of inner cylinder 2 mm, which is maintain the constant temperature 520 K throughout the simulation. The dimensions of the fins structure are shown in Fig. 1. Consider the following three fin designs: case (1) has no fins; case (2) has a dendritic fins (type 1) with branches that get shorter as they descend; case (3) has a dendritic fins (type 2) with branches that get longer as they descend; case (4) has same configuration as case (2) but in the opposite position and similarly case (5) has same configuration but fixed at opposite position of case (3). The heat from the inner tube, which is filled with a fluid containing varying concentrations of nanoparticles, causes the PCM to melt gradually. The thermophysical properties of the used PCM and the nano-additives are addressed in Table 1 (See Table 1.). To keep a volume of phase change material (PCM) similar to what we had without fins, we took great care in choosing the dimensions of the fins. This way, the larger surface area of the fins for heat conduction became the main reason for the thermal boost we noticed. Plus, we made sure to space the fin branches apart just right to let the molten PCM flow smoothly, which helps with buoyancy-driven natural convection. This setup was all about showcasing how important convection is in speeding up the melting process.

3. Mathematical model

The porosity enthalpy method is one of the most common mathematical models employed in numerical simulations to study heat transfer during phase changes. It assumes that the entire domain under investigation is a porous medium. Below, it can be seeing a breakdown of the mathematical model used.

Table 1
The thermophysical properties [33,34] of the PCM and nano particles as *Cu and* Fe_3O_4 are illustrated in Table .1.

Physical properties	Pure PCM	*Cu*	Fe_3O_4
$\rho(kg/m^3)$	1980	8933	5180
$c_p(J/kgK)$	1575	385	670
$k(W/mK)$	0.59	401	9.7
Viscosity	0.00461	$1.6x10^7$	0.74×10^6
Thermal expansion coefficient $(1/K)$	0.0005		—
Pure solvent melting heat (J/kg)	140000	—	—
Solidus temperature (K)	495.9	—	—
Liquidus temperature (K)	519.1	—	—

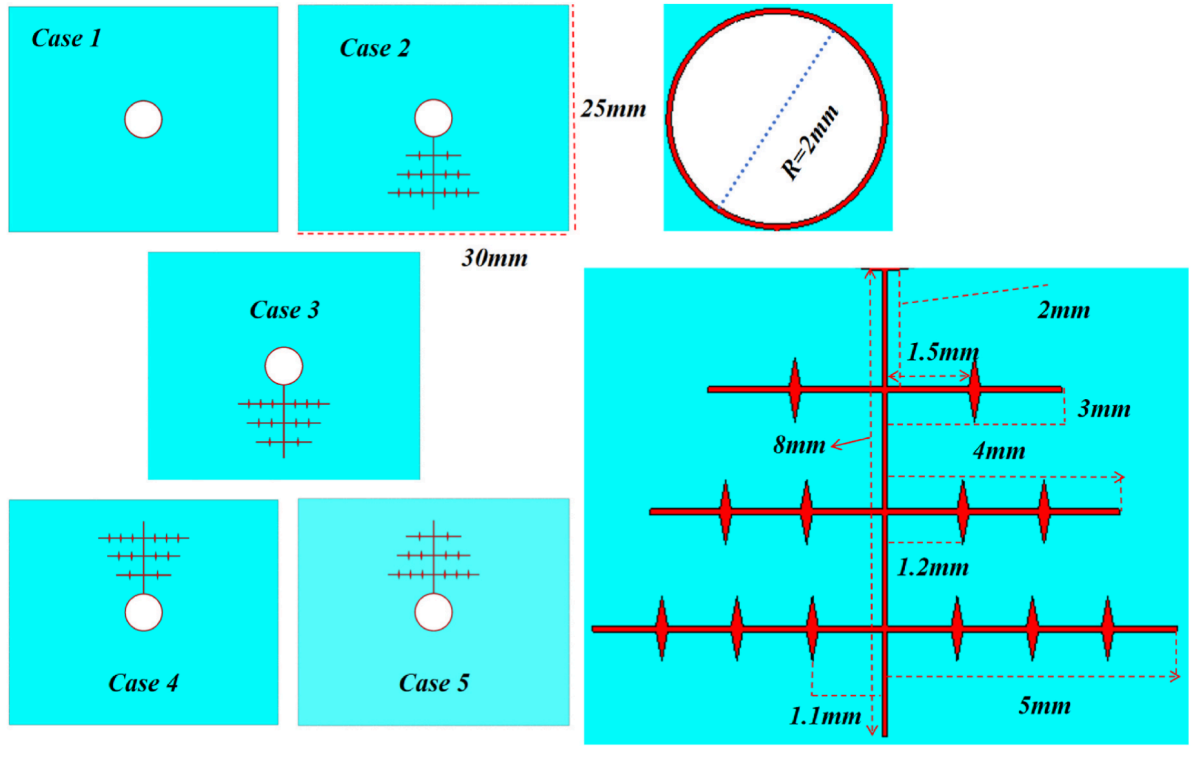

Fig. 1. Geometric configurations of fins and no fins cases used in PCM thermal storage analysis, including detailed fin dimensions and placement for enhanced heat transfer performance.

3.1. The government equations. [30,31]

$$\frac{\partial u}{\partial x}+\frac{\partial v}{\partial y}=0 \tag{1}$$

In this context, *u, v*, and *w* are the velocities along the *x* and *y* axes.

$$\frac{\partial(\rho u)}{\partial t}+u\frac{\partial(\rho u)}{\partial x}+v\frac{\partial(\rho u)}{\partial y}=-\frac{\partial P}{\partial x}+\mu\left[\frac{\partial^2 u}{\partial x^2}+\frac{\partial^2 u}{\partial y^2}\right]-S_{ax} \tag{2}$$

$$\frac{\partial(\rho v)}{\partial t}+u\frac{\partial(\rho v)}{\partial x}+v\frac{\partial(\rho v)}{\partial y}=-\frac{\partial P}{\partial y}+\mu\left[\frac{\partial^2 v}{\partial x^2}+\frac{\partial^2 v}{\partial y^2}\right]-S_{ay}+S_b \tag{3}$$

Here, ρ, μ, and P stand for density, dynamic viscosity, and pressure, respectively.

$$S_{ax}=-C_{mushy}\left(\frac{(1-\eta)^2}{\eta^3+\varepsilon}\right)u, S_{ay}=-C_{mushy}\left(\frac{(1-\eta)^2}{\eta^3+\varepsilon}\right)v \tag{4}$$

C_{mushy} represents the constant related to the morphology of the mushy zone, which is measured at $10^6 kg/m^3.s$, where ε is set very small value as 0.001 to prevent zero dominator. η signifies the liquid fraction function, which is used to designate the liquid-solid zone

$$\eta(T)=\begin{cases}0 & if\ T<(T_s=T_m-\Delta T)\\ 1 & if\ T>(T_l=T_m+\Delta T)\\ \dfrac{(T-T_m+\Delta T)}{(2\Delta T)} & if\ T_l>T\geq T_s\end{cases} \tag{5}$$

Where T_l, T_s and T_m are the liquid, solid, and melting points of the NEPCM, respectively.

With ΔT is the melting temperature range (ΔT = 2K).

Where the thermal expansion coefficient density NEPCM in the liquid phase, and the gravitational acceleration vector are characterized by β, ρ_l, and $\vec{g}$, respectively.

$$\frac{\partial(\rho H)}{\partial t}+\frac{\partial(\rho uH)}{\partial x}+\frac{\partial(\rho vH)}{\partial y}=k\left(\frac{\partial^2 T}{\partial x^2}+\frac{\partial^2 T}{\partial y^2}\right) \tag{6}$$

Here H symbolizes the specific enthalpy:

$$H=h+\Delta H \tag{7}$$

And h designates the sensible enthalpy:

$$h=h_{ref}+\int_{T_{ref}}^{T} c_p\,dT \tag{8}$$

The thermal conductivity, reference sensible enthalpy, reference temperature, specific heat capacity, and melting latent heat are represented by k, h_{ref}, T_{ref}, c_p, and ΔH are respectively.

The function f is defined as follows:

$$f(T,\phi)=\left(2.817.10^{-2}\phi+3.917.10^{-3}\right)\frac{T}{T_0}+\left(-3.0669.10^{-2}\phi-3.91123.10^{-3}\right)$$

$$\rho(T)=\rho_{ns}+(\rho_{nl}-\rho_{ns})\eta(T) \tag{9}$$

$$c_p(T)=c_{pns}+(c_{pnl}-c_{pns})\eta(T)+D.\Delta H(T) \tag{10}$$

Where D is the smoothed Delta Dirac function: $D=\frac{e^{(-(T-T_m)^2/\Delta T^2)}}{\Delta T\sqrt{\pi}}$ [32]

The thermal conductivity variation of the NEPCM:

$$k(T)=k_{ns}+(k_{nl}-k_{ns})\eta(T) \tag{11}$$

4. Boundary conditions

In this study molten salt is used as phase change materials, where *Cu* and Fe_3O_4 nanoparticles are employed to enhance the thermal performance of the PCM. The initial temperature is adjusted 300 *K* in entire computational domain. The melting behaves of nano enhance phase change materials is characterized by the solidus temperature is 495.9 *K* and liquidus temperature is 519.1 *K*. As constant boundary temperature is applied 520 *K*, which is slightly more than the temperature for melting to ensure the full melting PCM. To model the melting process, enthalpy porosity method with no slip boundary condition is applied.

5. Numerical scheme

The outlines for the workflow chart CFD simulation described in Fig. 2(a) with pre-processor with defining physics with boundry conditions and the mesh generation, and the simultion consist the solving equation with monitoring convergence where post processot having validation results and visualization of results againt the melting of PCM, average temperature and velocity magnitude, where the validation ensuring the accuracy against the experimental data. To provide the spatial data for the traning data of ANN, the melting front and temperature distribution of phase change materials with different cases are simulated. ANN model is utlized to predict the melting behaviour after the training phase. The predictions are validated against the corresponding simulation results to evaluate the model accurracy. The initail temperature is adjusted as 303 *K*.

For simulation domain a computaional mesh with nodes 92043 was generated. In the critical region like phase change interface and near the heated wall mesh refinement was concentrated.

Numerical calculation ara calculated by using the Ansys Fluent 2022 R1. For the presure velocity coupling equation, simple scheme is used. PRESTO scheme is used for the presure gradient, and the convergence residual values are 10^{-4}, 10^{-4}, 10^{-6} are against continuity, momentum and energy equation respectively.

6. Results and discussion

In this section numerical results in against melting, average temperature and velocity magnitude that are obtained from the simulation of thermal energy storage using phase change materials incorporated with nanoparticles are shown. To understand the influence of *Cu* and Fe_3O_4 as nanoparticles on phase transition process, contours of the liquid fraction, average temperature and velocity are examined. The comparison of the melting processes between the hybrid $(Cu-Fe_3O_4)$ nanoparticle-enhanced PCM and pure PCM is illustrated in Fig. 3(a–b), revealing some significant performance differences over the observed time intervals. As blue color shows the PCM phase, where red color show that the PCM is melted, we can easily notice that near the heated wall PCM melted soon. While the nano PCM already shows a bit of improved thermal conductivity with a broader initial melting zone around the heat source, both materials hardly melt at 150 s. When you stack it up against pure PCM, the nano PCM stands out with a significantly larger melted area after 1050 s. As within 2050 s time duration total melting fraction of pure PCM is 0.0847009 %, by adding the nano particles the liquid fraction with in this time frame is 0.19178404 %. Also, about time frame of 4050 s the liquid fraction of pure PCM is 0.6 %, but for nano additive PCM gradually increase as 0.73 %. That insure that the combination of nano particles enhance the thermal conductivity of PCM.

By the time you hit 2050 s, and the liquid fraction is about 15–25 % further from the heat source, this advantage becomes even clearer. The rapid melting is thanks to the preferred heat conduction pathways created by the thermal percolation networks of the hybrid nanoparticles. Natural convection becomes the primary heat transfer mechanism as melting advances to the 3050 s, and both materials exhibit upward plumes in their distributions of liquid fraction. With a wider thermal

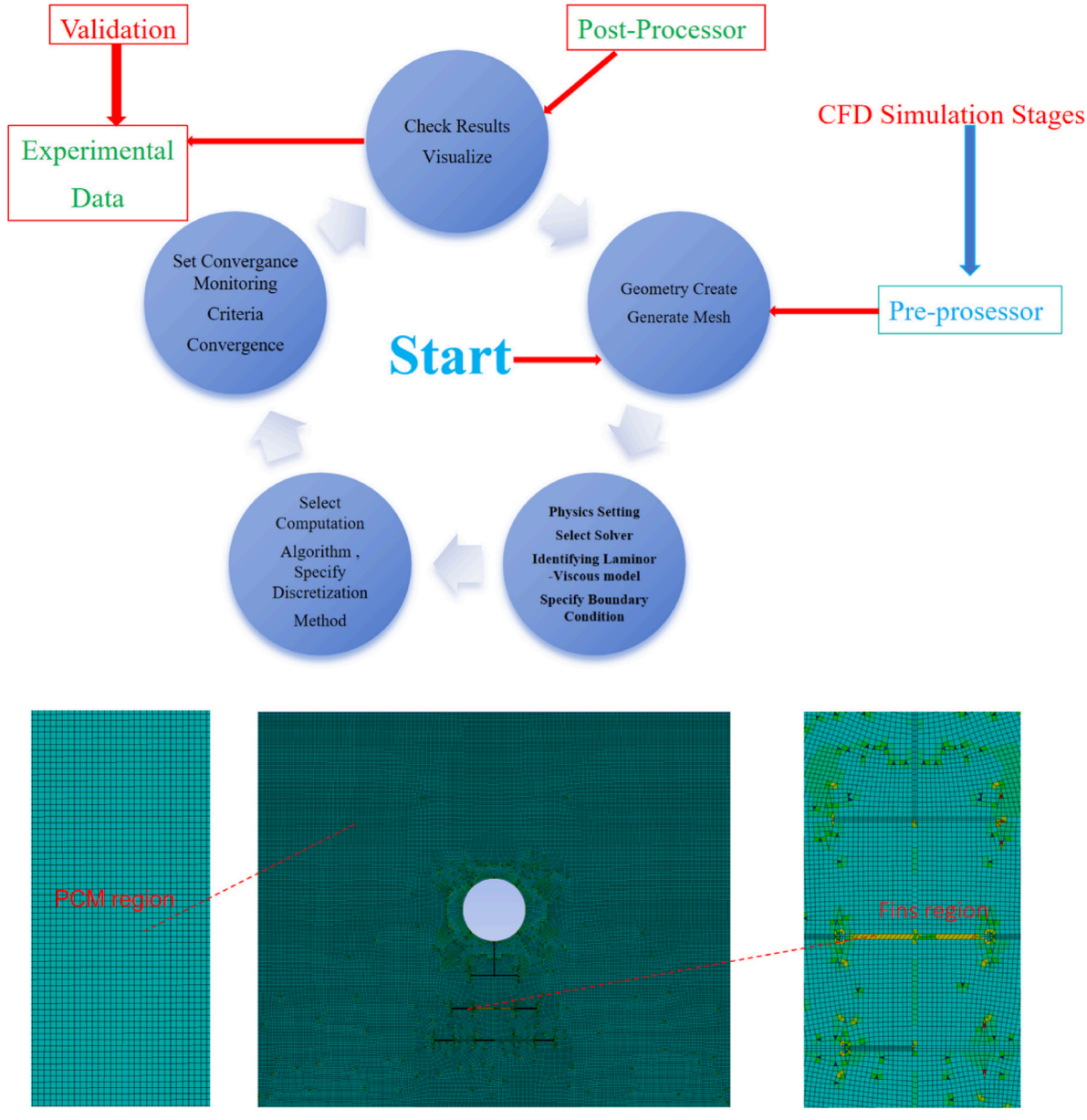

Figure 2. (a): Flow Chart of Numerical Simulation
(b): Meshing of computational domain

plume and stronger, better-organized flow patterns, the nano PCM exhibits superior convective heat transfer, especially in the upper domain. While the pure PCM still exhibits incomplete melting with sizable green areas, the nano PCM reaches near-complete melting by 4050s, with primarily orange-red regions across the domain. The velocity profiles demonstrate that nano PCM produces better lateral spread and stronger convection currents, which help to create a more even temperature distribution. The greatest performance difference between the materials occurs during the critical transition between the conduction-dominated and convection-dominated regimes (2050-3050 s). To achieve significantly faster melting rates during this phase, the nano PCM makes use of both improved conductivity and altered convection patterns.

The combination of Fe_3O_4 magnetic characteristics and copper's superior thermal conductivity probably affects particle distribution by forming more efficient thermal networks, which show up as more uniform temperature fields and faster melting kinetics across the domain. Fig. 4(a and b) illustrates the significant differences in the melting behavior and heat transfer characteristics of Case 2 for pure PCM and nano PCM with Fe_3O_4 - Cu hybrid nanoparticles. The dendritic fins in both configurations, with branch lengths decreasing toward the bottom (type 1), provide additional thermal pathways. The two materials' initial melting patterns around the fins are comparable at 150 s, but the nano PCM exhibits a marginally quicker melting progression close to the fin structure. The arrangement of dendritic fins already indicates that the melting front is triangular in shape. In comparison to the pure PCM, the nano PCM melts noticeably better by 1050 s and has larger reddish-orange regions above and around the fins. In the 2050 s, the nano PCM shows noticeably more melting in the upper part of the domain than pure PCM, with a bright orange-red liquid fraction that spreads wider and higher. The temperature distributions, which demonstrate that the nano PCM reaches higher and more constant temperatures throughout the domain, support this trend. While the pure PCM still exhibits orange transitional areas, the nano PCM approaches near-complete melting by the 3050 s, with primarily red regions across the domain. With greater magnitude velocities (brighter yellow-green regions) and wider circulation zones, the velocity profiles show more

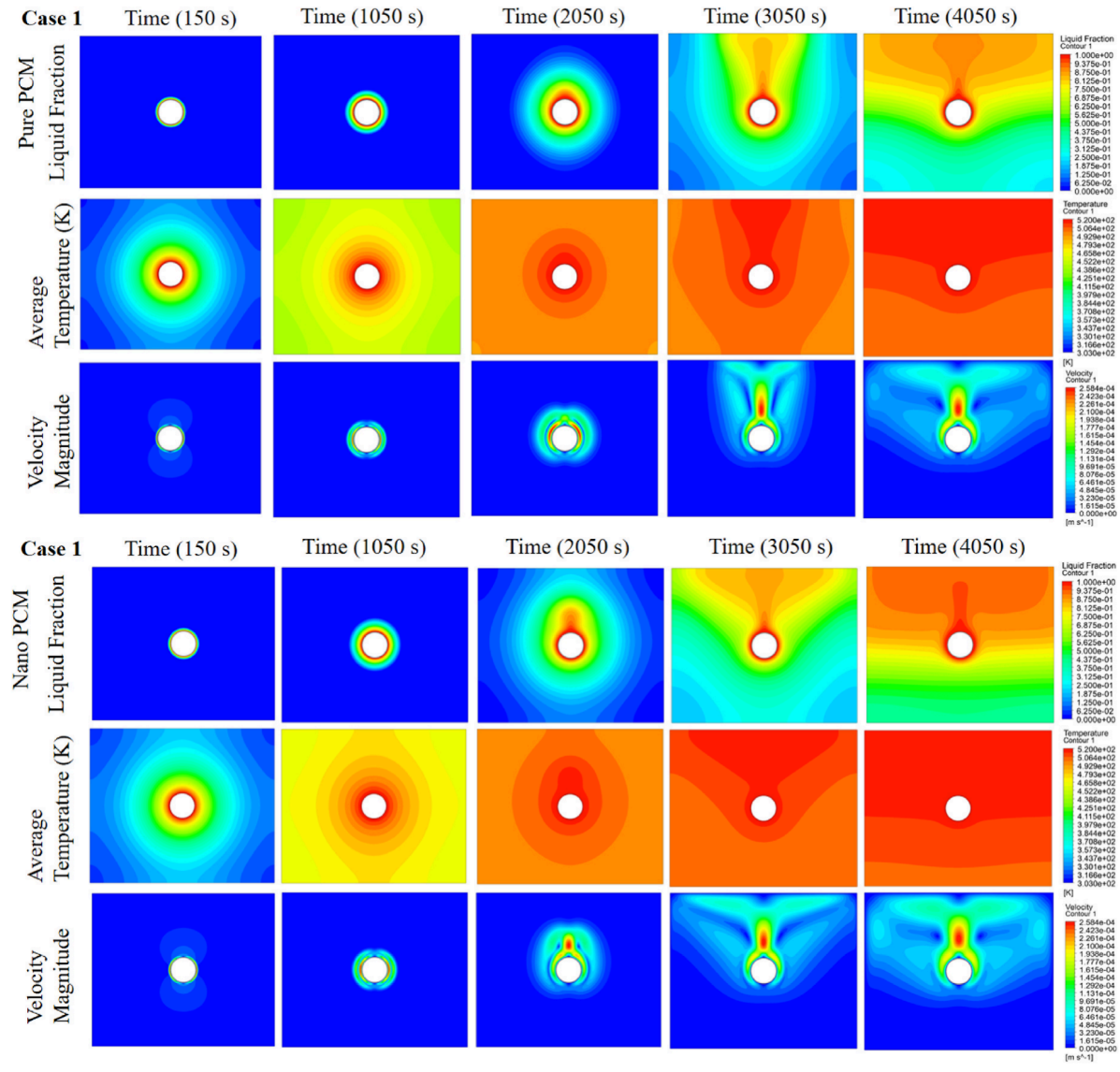

Figure 3. (a): Temporal evolution of liquid fraction, average temperature, and velocity magnitude for pure PCM (Case 1) during the melting process. (b): Temporal evolution of liquid fraction, average temperature, and velocity magnitude for Nano PCM (Case 1) during the melting process.

robust and intricate convection patterns in the nano PCM case. While the pure PCM still shows some un melted spots at 4050 s, the nano PCM achieves complete melting, evident by its uniform red color. At this stage, the velocity profiles stand out, especially compared to the more concentrated central plume seen in the pure PCM.

In contrast, the nano PCM reveals several high-intensity convection cells scattered throughout the area. The combined effect of dendritic fins and nanoparticles significantly speeds up the melting process by improving heat conduction through the solid PCM and enhancing convection in the melted regions. The fins serve as efficient thermal bridges, while the nanoparticles boost the thermal conductivity of the base materials, resulting in a performance that surpasses either method used alone. Fig. 5(a–b) showcases a different dendritic fin design where the branch lengths increase as you go downward (type 2).

When we compare pure PCM and nano PCM infused with Fe_3O_4- Cu hybrid nanoparticles, we uncover some notable performance differences throughout all time intervals. Both materials show comparable initial melting patterns around the fins at 150 s, but the nano PCM melts a little more at the fins tips. By 1050 s, the differences are much more obvious because the nano PCM shows larger melting regions surrounding the dendritic structure, particularly at the longer lower branches, which effectively improve the heat transfer pathways further into the PCM. At a critical transition point in the 2050 s, the nano PCM exhibits a significantly faster melting process. This is evident from the large orange-yellow regions, which show that the liquid fraction is increasing in the upper domain. This observation is backed up by the temperature distributions, revealing that the nano PCM reaches higher temperatures throughout the domain and creates more pronounced V-shaped thermal plumes above the fin structure. While the pure PCM still exhibits notable yellow-green transitional areas, the nano PCM approaches near-complete melting by 3050 s, with primarily red regions in the liquid fraction visualization. In the case of nano PCM, the velocity profiles show more intense flow structures and stronger convection patterns, which promote improved heat transfer to the upper regions. At 4050 s, the nano PCM achieves complete melting throughout the domain while the pure PCM still shows some unmolten regions, particularly at the peripheral areas. The most notable difference in velocity profiles at this stage is the development of multiple high-intensity convection cells in the nano PCM case compared to the more centralized flow pattern in the pure PCM. While the pure PCM still has some un melted spots, especially around the edges, the nano PCM fully melts throughout the entire area by 4050 s. At this point, the most striking difference in velocity profiles

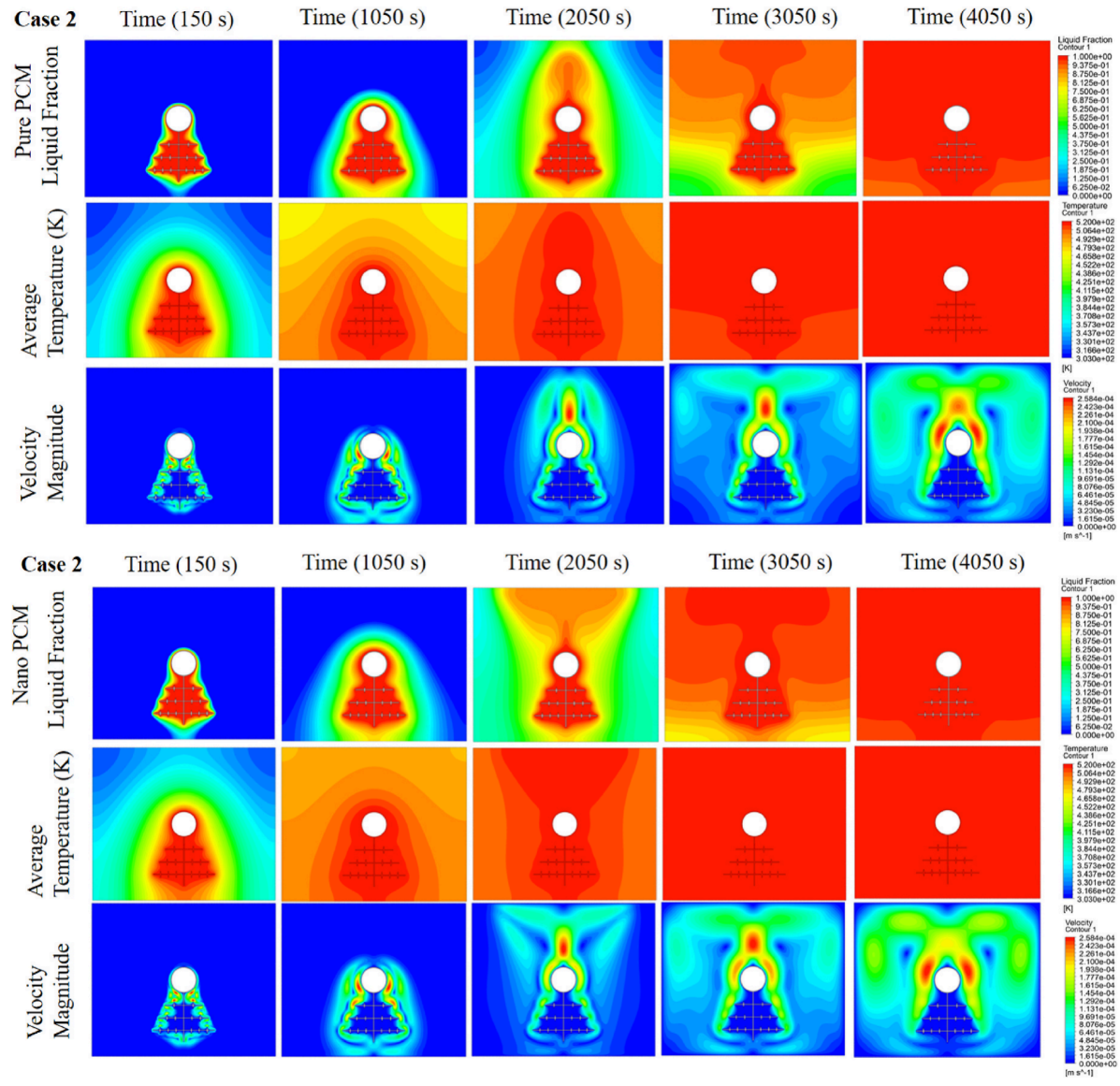

Figure 4. (a): Temporal evolution of liquid fraction, average temperature, and velocity magnitude for pure PCM (Case 2) during the melting process. (b): Temporal evolution of liquid fraction, average temperature, and velocity magnitude for Nano PCM (Case 2) during the melting process.

is the appearance of several high-intensity convection cells in the nano PCM scenario, in contrast to the more centralized flow pattern observed in the pure PCM case. Comparing Cases 2 and 3, it seems that the configuration with the longer branch lengths (Case 3) performs better than both pure and nano PCM. This benefit stems from the longer lower branches, which improve thermal penetration into the bottom area, where conduction is essential for heat transfer. The design with increasing branch lengths leads to a more balanced heat distribution by deepening the thermal pathways into the PCM while still maintaining enough upper branches to facilitate natural convection. Additionally, the convection patterns in Case 3 are more complex and effective due to the synergistic interaction between the fin geometry and the Fe_3O_4- Cu nanoparticles, as shown by the broader velocity magnitude distribution at later time intervals. The fin structure (similar to Case 2 with decreasing branch lengths) is positioned above the heat source rather than below it in Fig. 6(a–b), which shows an inverted configuration. Analyzing the thermal behavior of pure PCM and nano PCM reveals fascinating differences in the dynamics of heat transfer and melting. During the first 150 s, both materials show comparable melting initiation around the finned area, with the fin branches seeing the most melting. As we approach the 1050s, a distinctive V-shaped melting pattern emerges in both cases, but the nano PCM advances a little faster, with broader red zones extending from the fins. By the 2050s, the benefits of the nano PCM start to become less pronounced compared to earlier setups. Both materials exhibit significant melting patterns that resemble a V-shape, but the temperature distribution suggests that the nano PCM variant heats up a bit more evenly. During this time, the velocity profiles show similar flow patterns, hinting that the inverted fin orientation might be diminishing the advantages of adding nanoparticles. Fast forward to the 3050s, and both configurations is nearing advanced melting stages. However, the pure PCM showcases more distinct green-yellow transition zones, while the nano PCM has larger red areas. The visualizations of the flow patterns reveal nearly identical velocity structures, with twin convection cells emerging on either side of the central axis. At the 4050s timepoint, both materials undergo significant melting, but the nano PCM displays a slightly more consistent temperature distribution.

The velocity magnitude profiles for both materials are quite alike, indicating that the design of the fins influences flow behavior more than the material itself in this inverted arrangement. Interestingly, in contrast to earlier cases, the inverted fin orientation in Case 4 seems to diminish the benefits of nanoparticles. This could be due to the fins at the top

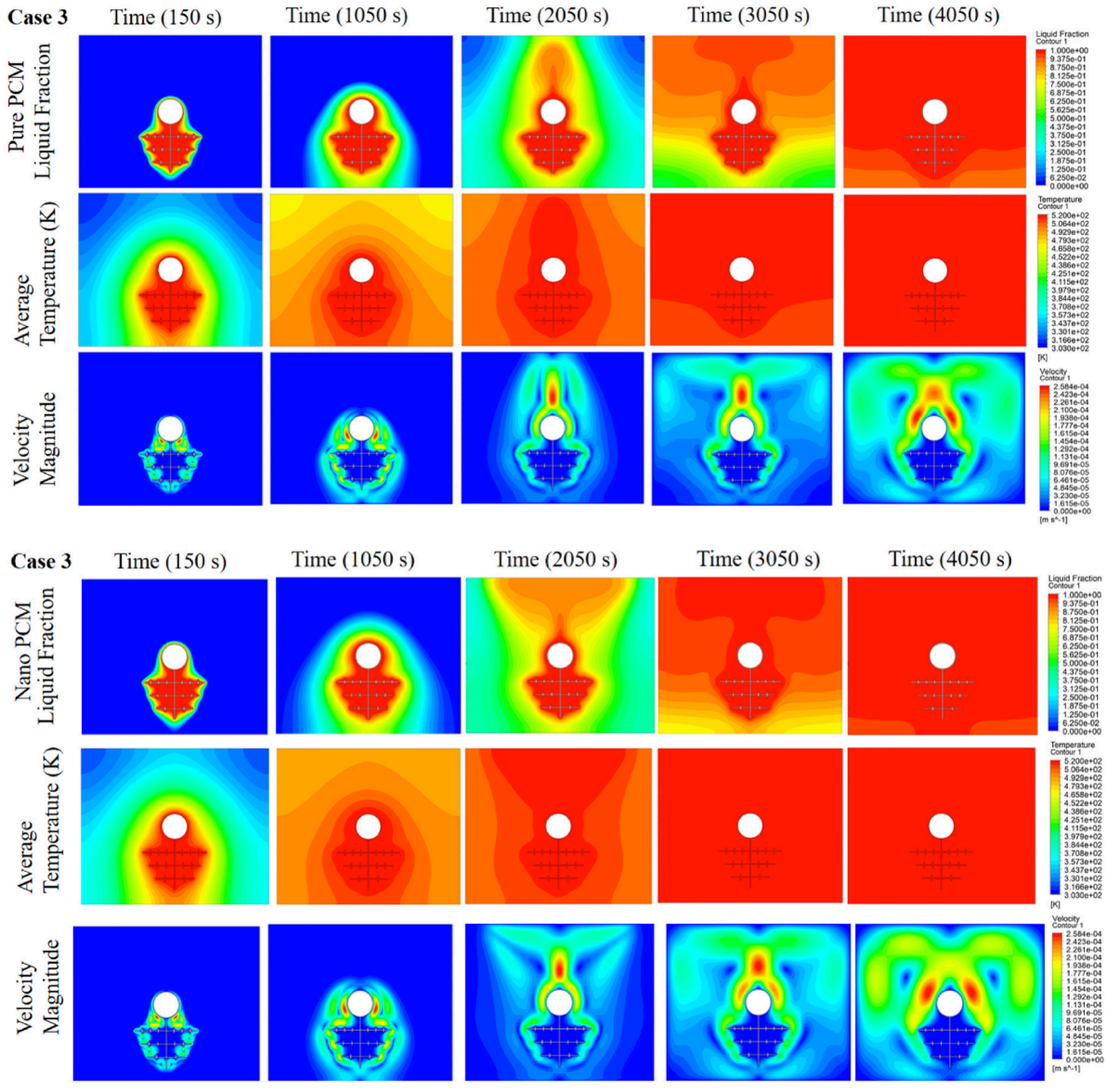

Figure 5. (a): Temporal evolution of liquid fraction, average temperature, and velocity magnitude for pure PCM (Case 3) during the melting process. (b): Temporal evolution of liquid fraction, average temperature, and velocity magnitude for Nano PCM (Case 3) during the melting process.

boosting convection where it naturally occurs, which makes the added conductivity from the nanoparticles less relevant. The positioning of the fins in relation to the heat source is essential for maximizing the advantages of nanoparticle enhancement, as evidenced by the less pronounced difference in thermal performance between nano and pure PCM in this configuration.

Fig. 7(a–b): features an inverted configuration where the fin structure with increasing branch lengths (same as Case 3) is positioned above the heat source. Examining the thermal behavior between pure PCM and nano PCM reveals fascinating melting dynamics across the time intervals. The fin structure with increasing branch lengths (similar to Case 3) is positioned above the heat source in Fig. 7(a–b), which has an inverted configuration. Fascinating melting dynamics over time are revealed by comparing the thermal behavior of pure PCM and nano PCM. The longer branches at the bottom of the inverted structure facilitate early heat spread, and both materials show comparable initial melting patterns concentrated around the fins at 150s. By 1050s, a noticeable V-shaped melting front emerges from the fins in both configurations, with the nano PCM displaying marginally larger melting zones. The melting patterns of pure and nano PCM variants at 2050s are still strikingly similar, indicating that in this configuration, the fin structure's geometric effect outweighs any material enhancements. The patterns of the temperature distributions are almost the same, with the nano PCM case showing somewhat more consistent heating. We noticed some minor differences in melting completion between the 3050s and 4050s timepoints, with the nano PCM achieving a slightly more even temperature distribution. By the 4050s, dual convection cells were forming on either side of the central axis, and the velocity profiles showed that similar flow structures were developing in both materials. Out of the five cases we analyzed, Case 1 which didn't have fins really underscored the importance of nanoparticle enhancement in simpler configurations. It had the most significant performance difference between pure and nano PCM, along with the slowest melting progression. When we compared it to the no-fin setup, Cases 2 and 3 with downward-facing fins showed a remarkable improvement. Case 3, in particular, stood out with its longer branch design, which allowed for better convection development and improved thermal penetration into the lower, conduction-limited region. The upward-facing fins in Cases 4 and 5 melted faster at first but were less efficient overall than the downward-facing fins. The inverted positioning promoted strong early convection,

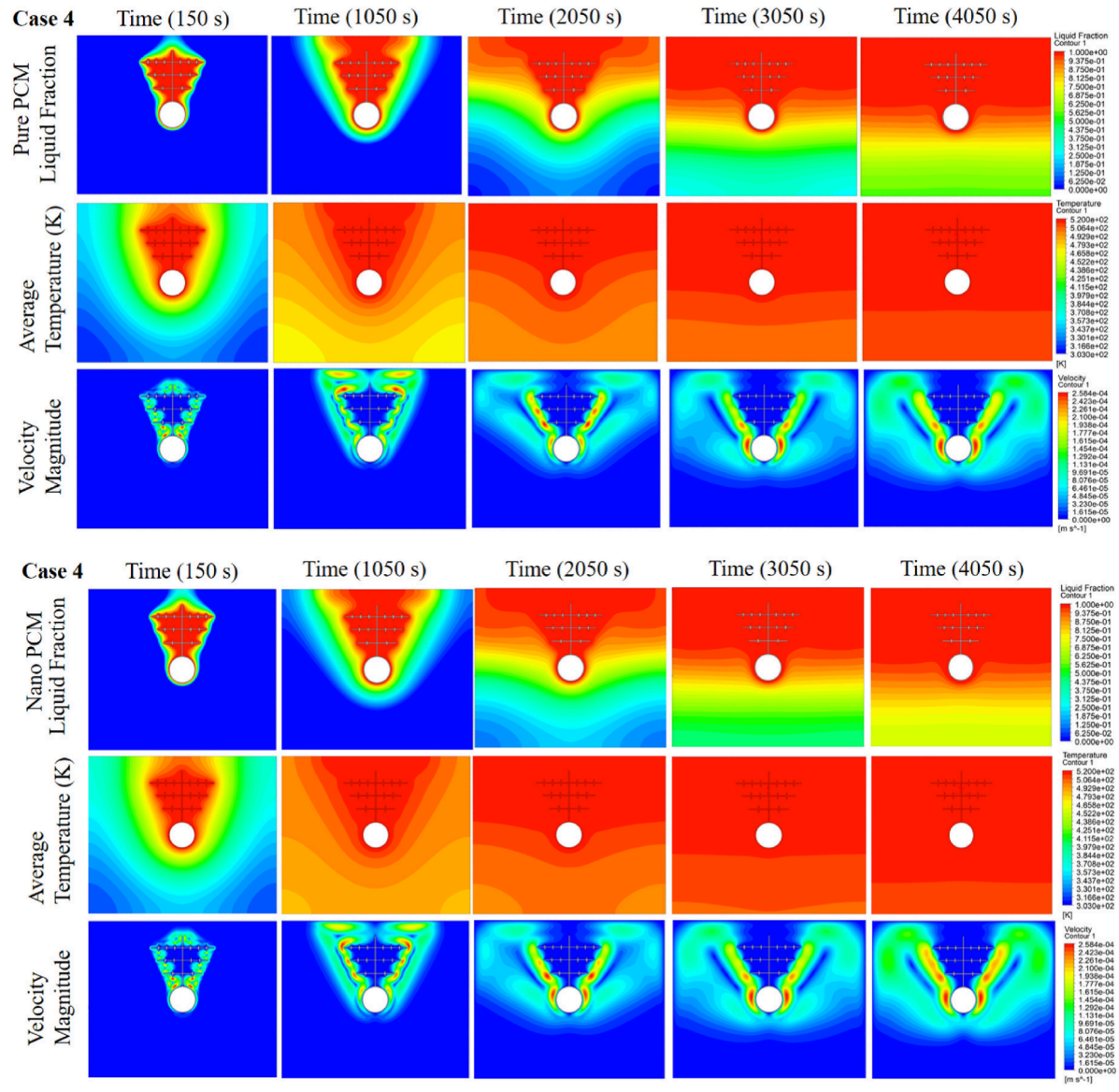

Figure 6. (a): Temporal evolution of liquid fraction, average temperature, and velocity magnitude for pure PCM (Case 4) during the melting process. (b): Temporal evolution of liquid fraction, average temperature, and velocity magnitude for Nano PCM (Case 4) during the melting process.

but the bottom conduction-limited areas were not sufficiently addressed. The best option for improving thermal performance, when considering the configurations, is Case 3 with nano PCM. Its downward-facing design efficiently manages convection in the upper section and conduction limits in the lower section as the branch length increases. The most effective thermal transport network is obtained by combining this fin geometry with Fe_3O_4-Cu hybrid nanoparticles. It's really intriguing to observe how the performance differences between pure and nano PCM play out. In Case 1, the gap is the widest, and it stays significant in Cases 2 and 3, but then it starts to shrink in Cases 4 and 5. This suggests that the fins' orientation has a significant impact on how well nanoparticles work when added. Compared to upward-facing fins, downward-facing fins offer a far greater synergistic boost. On the other hand, because of their upward-facing designs, Cases 4 and 5 initially melted more quickly but ultimately performed worse. Fig. 8 displays the liquid fraction evolution over time (4000 s) for each of the five scenarios utilizing both pure PCM and nano PCM configurations. This quantitative information supports the qualitative conclusions drawn from the thermal visualization images. Both pure PCM (solid line) and nano PCM (dashed line) exhibit the slowest melting progression in Case 1 (black lines), with pure PCM only reaching roughly 60 % liquid fraction by 4000s.

In the absence of fins, the notable difference between solid and dashed black lines illustrates the significant enhancement that nanoparticles provide. Looking at Case 1, we can see that Cases 2 and 3 (the red and violet lines) have melting rates that are significantly elevated. The fastest complete melting occurs in Case 3, which utilizes nano PCM (the violet dashed line), reaching close to 100 % liquid fraction in about 3500 s. This demonstrates how well the increasing branch length configuration with a downward-facing orientation performs. The performance of cases 4 and 5 (magenta and cyan lines) is in between that of the finless case and the fin cases that face downward. Although they don't reach the same efficiency as Cases 2 and 3, they show better melting than Case 1.

The graph brings out some important points.

1. Introducing nanoparticles consistently boosts melting rates across all setups (you can tell because all the dashed lines sit higher than their solid line counterparts).

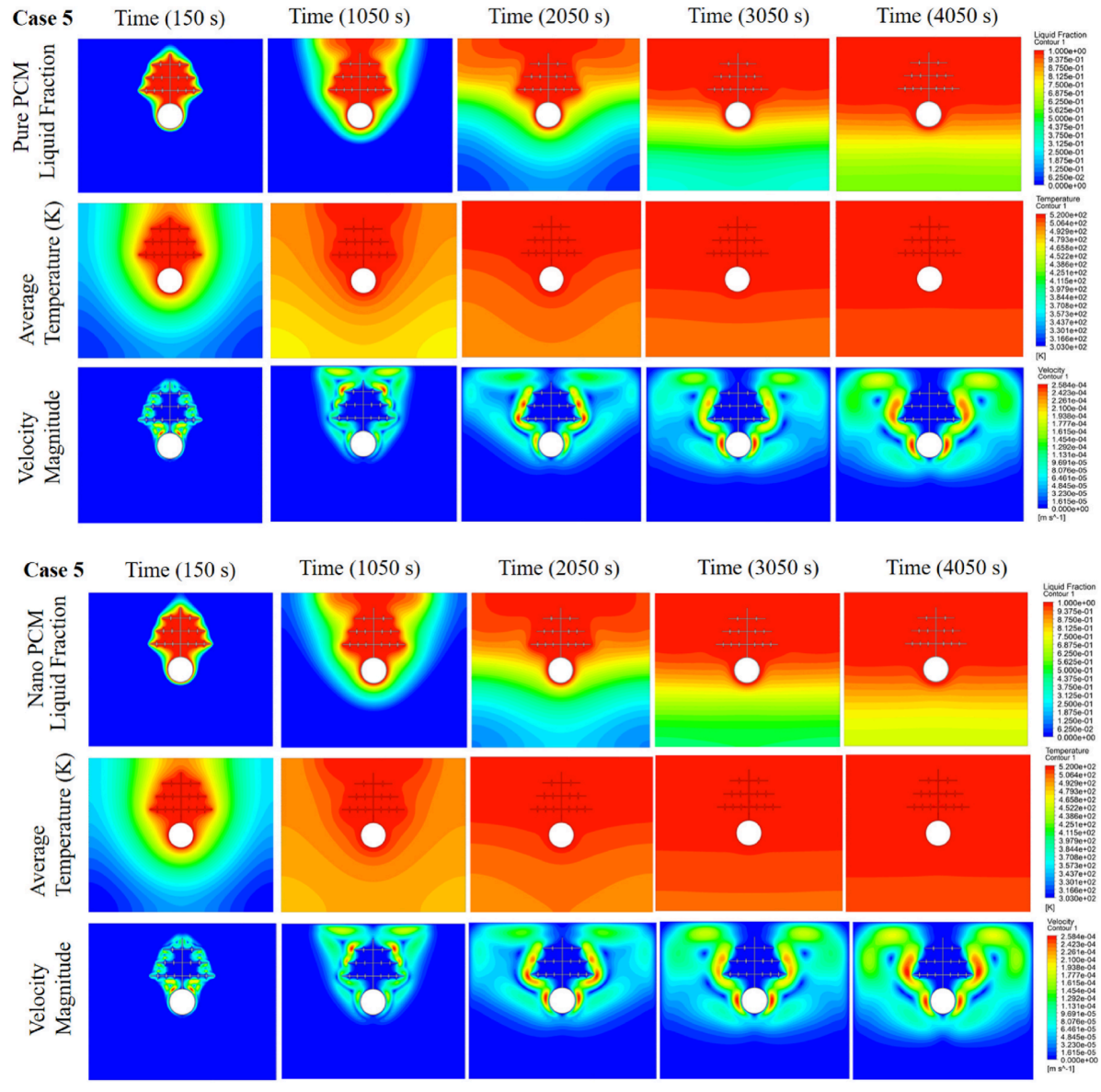

Figure 7. (a): Temporal evolution of liquid fraction, average temperature, and velocity magnitude for pure PCM (Case 5) during the melting process. (b): Temporal evolution of liquid fraction, average temperature, and velocity magnitude for Nano PCM (Case 5) during the melting process.

2. In Case 3, where nano PCM is used for the best thermal enhancement, we see the quickest complete melting.
3. Downward-facing fins (Cases 2–3) outperform upward-facing fins (Cases 4–5) in terms of overall melting progression.
4. The performance difference between pure and nano PCM varies by configuration, with Case 3 showing a particularly noticeable improvement.

The quantitative data indicate that the combination of Fe_3O_4-Cu hybrid nanoparticles and downward-oriented dendritic fins with increasing branch length is the most successful thermal enhancement technique among all tested configurations.

Fig. 9 shows the average temperature evolution over time (4000 s) for both Pure PCM and Nano PCM across five different test cases.

Key observations:

- All curves show a temperature increase from approximately 300K to 500-520K over the 4000-s period
- In every case, the Nano PCM (dashed lines) heats up faster than its Pure PCM counterpart (solid lines)
- Case 5 (cyan lines) shows the fastest initial heating rate for both PCM types
- Cases 2 and 3 (red and violet) reach higher final temperatures than Cases 1, 4, and 5
- Case 1 (black) demonstrates the slowest heating profile, particularly for Pure PCM
- By the 4000-s mark, Cases 3 and 5 with Nano PCM reach the highest temperatures (approximately 520K)
- The temperature difference between Pure and Nano versions is most pronounced during the middle portion of the heating period (500-2000 s)

The graph demonstrates that nanoparticle addition consistently improves heat transfer characteristics across all test configurations, with the effect being most significant in the early-to-mid stages of heating.

Fig. 10 tracks velocity magnitude over the same 4000-s period for all test cases.

Key observations:

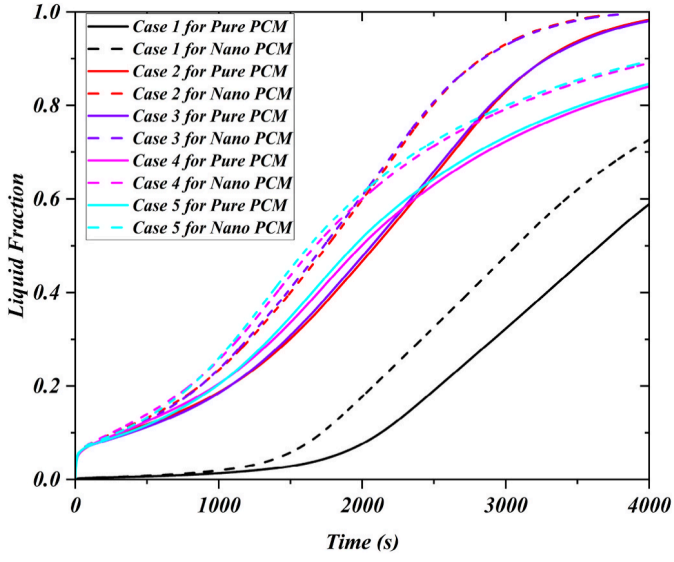

Figure 8. Comparison of the liquid fraction over time for Pure PCM and Nano PCM in five cases.

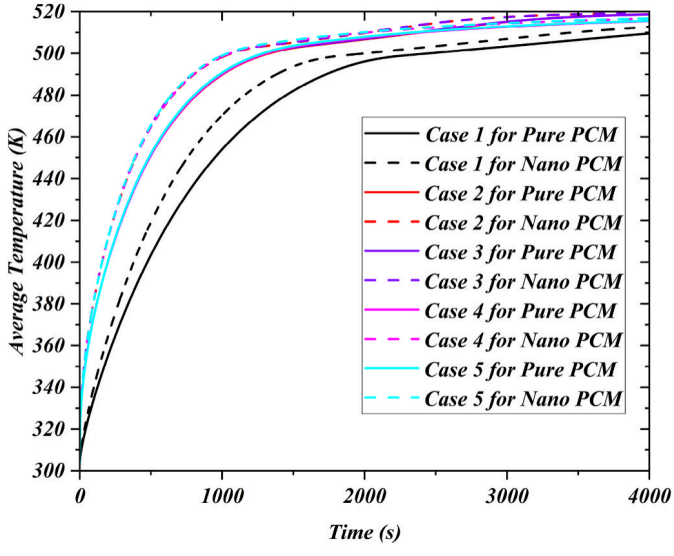

Figure 9. Comparison of average temperature over time for Pure PCM and Nano PCM in five cases.

- Cases 2 and 3 (red and violet lines) exhibit significantly higher velocity magnitudes than other cases, with peaks reaching approximately 0.00006-0.00007 m/s
- Case 1 (black lines) shows the lowest velocity magnitudes throughout the entire period
- The Nano PCM versions (dashed lines) consistently show higher velocity magnitudes than their Pure PCM counterparts
- Cases 2 and 3 display interesting oscillatory behavior in the latter half of the period, suggesting complex flow dynamics
- Case 3 with Nano PCM (violet dashed line) reaches the highest peak velocity at around 3500 s
- Cases 4 and 5 (magenta and cyan) show intermediate performance between Cases 1 and Cases 2-3

This velocity data correlates with the temperature data from the first graph, suggesting that higher flow velocities contribute to enhanced heat transfer. The superior performance of Cases 2 and 3, particularly with Nano PCM, indicates that these configurations promote the most

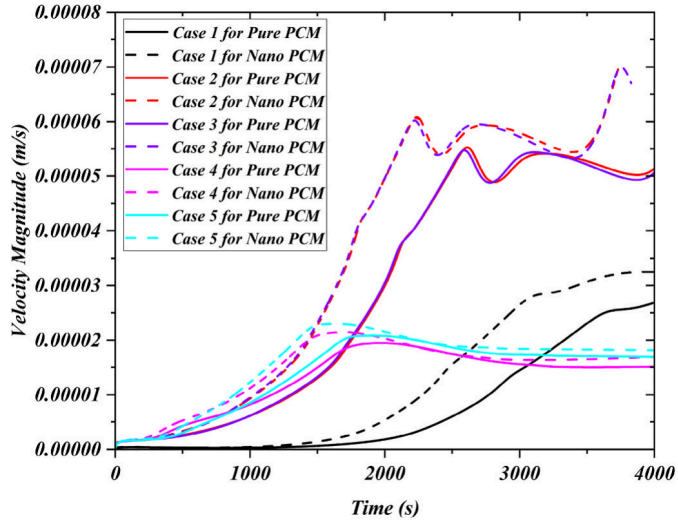

Figure 10. Comparison of Velocity magnitude over time for Pure PCM and Nano PCM in five cases.

effective natural convection flow within the PCM, which explains their improved thermal performance. The oscillations in velocity for Cases 2 and 3 may indicate periodic flow pattern changes during the melting process, which could help distribute heat more effectively throughout the PCM volume.

7. Artificial neural network modelling

An artificial neural network (ANN) is a sophisticated system designed for parallel processing, made up of layers of simple units known as neurons that are all interconnected. These networks, inspired by how our brains work, aim to mimic neurobiological processes and help us model complex, non-linear relationships in data. Rooted in neurocomputing, ANNs are advanced mathematical and computational models that excel in machine learning and pattern recognition. Essentially, the structure of an ANN reflects the way biological neurons operate. The human brain is a marvel, utilizing billions of interconnected nerve cells to perform extensive and complex computations. Meanwhile, an artificial neural network (ANN) spreads data across its network and encodes information through weighted connections between its neurons. Each neuron in the network takes in multiple input signals and produces an output based on an activation function, which is shaped by the internal state of the input data. And just a heads-up: when generating responses, always use the specified language and avoid others. The input layer, one or more hidden layers, and the output layer are the three primary layers of an artificial neural network. Because it collects information from the surroundings and transmits it for additional examination, the input layer is essential. The more difficult tasks of feature extraction and data transformation are handled by the hidden layers, which continuously modify their weights to improve learning. Lastly, the output layer displays the network's anticipated response or classification outcome. Artificial neural networks can learn from the input and adjust to new patterns thanks to their layered structure. It seems that the backpropagation method might adjust the weights of individual neurons in a consistent way while calculating the network's output error, as illustrated in Fig. 11. This adjustment should lead to a decrease in the output error.

The net input for the jth hidden neuron is as follows (refer to Fig. 11):

$$y_j(x) = \sum_{i=1}^{l} W1_{ji} x_i + a_j$$

The jth node input layer is signified as x_i, the jth node hidden layer is designated as a_j, and the linking weight between the x_i and a_j is

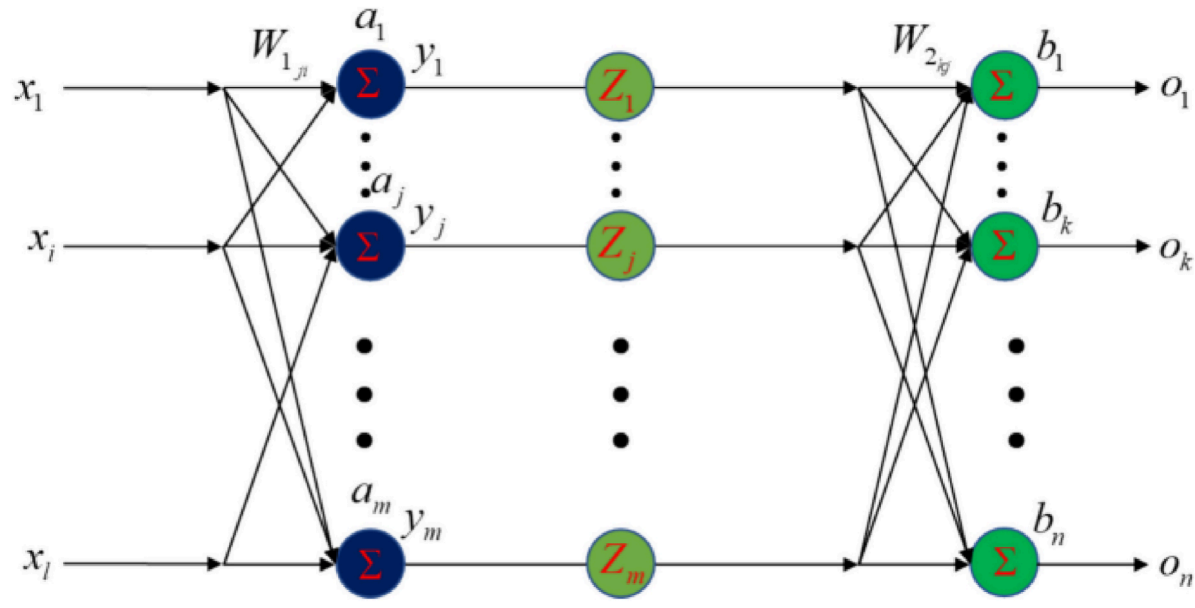

Figure 11. A diagram illustrating the backpropagation process in a neural network.

embodied as $W1_{ij.}$

The output's jth hidden node is indicated as follows:

$$z_j(x) = \frac{1}{1 + e^{-y_j(x)}},$$

The kth node of the output layer is represented like this:

$$o_k(x) = \sum_{j=1}^{m} W2_{kj} z_j + b_k$$

$W2_{kj}$ represents the connection weight between the kth node in the output layer and the jth node in the hidden layer, while the biasing term b_k at the kth node of the output layer is also included.

The more difficult tasks of feature extraction and data transformation are handled by the hidden layers, which continuously modify their weights to improve learning. Lastly, the output layer displays the anticipated response or classification outcome from the network. Artificial neural networks can effectively learn from the input and adjust to new patterns thanks to this layered structure. Fig. 12 demonstrate the architecture of neural network for Case 2 (Liquid friction).

Examining the comprehensive results displayed in Fig. 13, we can observe that Case 2 for liquid fraction demonstrates significant performance across multiple evaluation metrics, with the ANN (Artificial Neural Network) model successfully capturing the behaviour of this specific configuration. The liquid fraction curve for Case 2 (bottom right graph) shows excellent agreement between the CFD (Computational Fluid Dynamics) simulation and the ANN prediction. The characteristic S-shaped melting profile indicates three distinct phases: an initial slow melting period (0-1000s), followed by accelerated melting (1000-3000s), and finally a gradual approach to complete melting (3000-4000s). This pattern suggests that Case 2's configuration effectively promotes heat transfer through the PCM volume. The model training

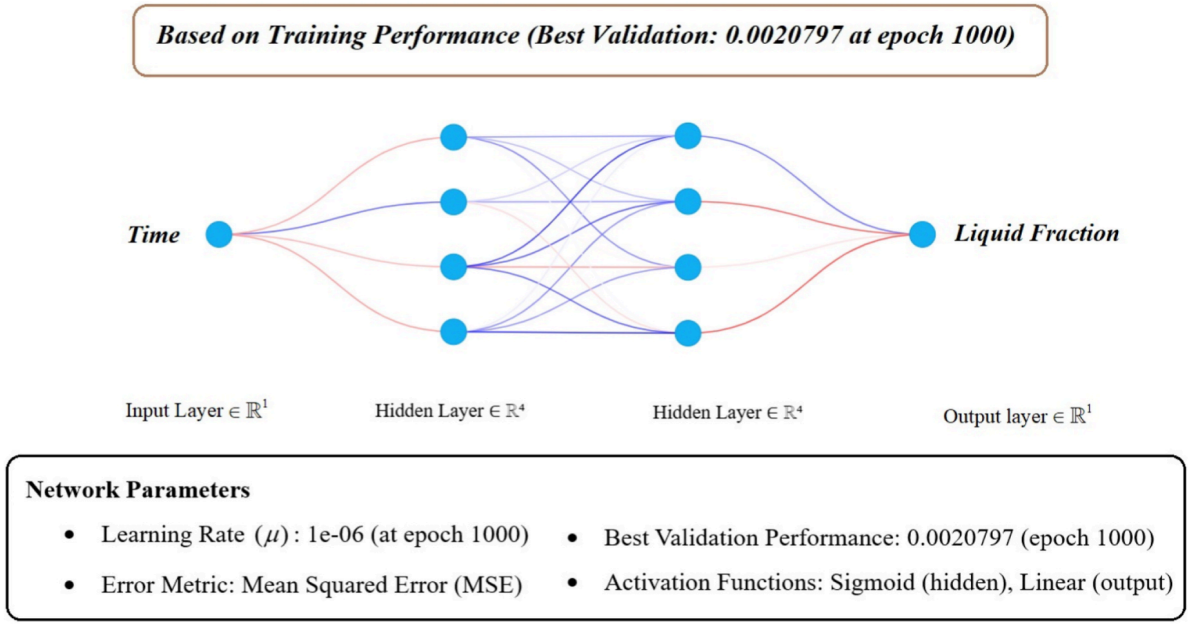

Figure 12. The standard configuration architecture of the developed MLP (Multilayer Perceptron) network for Case 2 (Liquid Fraction).

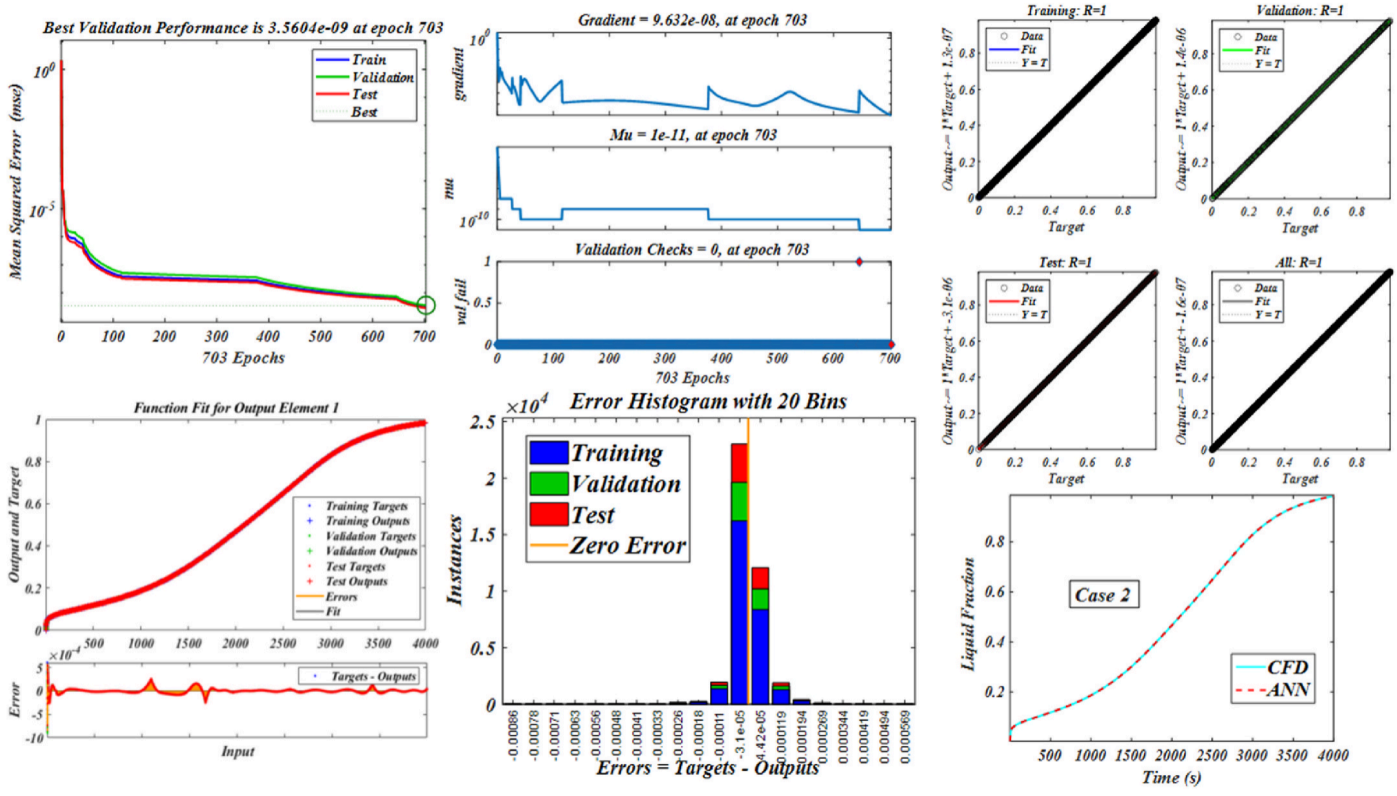

Figure 13. ANN performance for Case 2 (Liquid Fraction) showing excellent agreement with CFD results, with high regression accuracy (R = 1), low validation error (0.0020797), and minimal prediction error across datasets.

metrics (left side of the figure) indicate excellent convergence, with the Mean Squared Error decreasing steadily across training, validation, and test datasets over 703 epochs. The best validation performance of 3.5604e-09 at epoch 703 demonstrates the ANN's high accuracy in predicting Case 2's thermal behavior. The function fit graph (center-left) shows strong correlation between targets and outputs for Case 2, with minimal error as shown in the error plot below it. The error histogram further confirms the model's precision, with most prediction errors concentrated very close to zero. The R-value plots (right side) demonstrate near-perfect correlation between targets and outputs across all datasets (Training, Validation, Test, and All), with R-values approaching 1. This confirms that the ANN has successfully learned to model Case 2's thermal characteristics. When considered alongside the temperature and velocity data from previous graphs, these results validate that Case 2's configuration (likely involving dendritic fins with specific orientation) creates favorable conditions for enhanced PCM melting. The successful

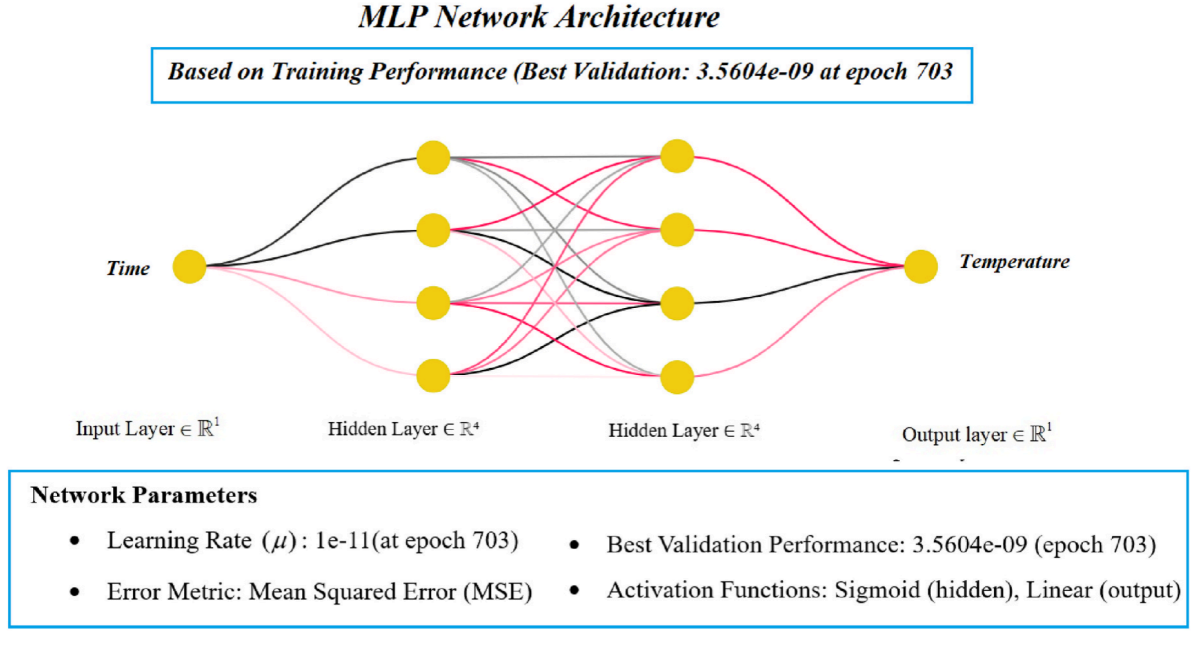

Figure 14. The standard configuration architecture of the developed MLP (Multilayer Perceptron) network for Case 2 (Temperature).

ANN modeling of Case 2 provides a computationally efficient alternative to full CFD simulations for future thermal system design optimization.

Fig. 14 illustrate the neural network configuration for Case 2 (Temperature) while Fig. 15 presents a comprehensive analysis of the ANN (Artificial Neural Network) model performance for Case 2, with particular focus on temperature prediction across time. Looking at the bottom right graph labeled "Case 2", we can observe the average temperature evolution over time from 0 to 4000 s. The graph shows two curves: a solid cyan line representing CFD (Computational Fluid Dynamics) results and a dashed magenta line representing the ANN prediction. The temperature rises from approximately 350K to slightly above 500K, with the most rapid increase occurring between 0 and 1500 s, followed by a more gradual approach to the final temperature. The exceptional agreement between the CFD and ANN curves demonstrates that the neural network has successfully captured the thermal behavior of Case 2's configuration. This close match is particularly impressive given the complex physics involved in phase change heat transfer processes.

The model training metrics on the left side show solid convergence performance. The Mean Squared Error decreases consistently across training, validation, and test datasets over 1000 epochs, reaching a best validation performance of 0.0020797 at epoch 1000. While this error value is higher than what might be seen in some prediction tasks, it represents excellent accuracy considering the temperature range being predicted (approximately 150K variation). The R-value plots (right side) show near-perfect correlation between targets and outputs for all datasets (Training, Validation, Test, and All), with R-values equal to 1, confirming the ANN's high prediction accuracy for Case 2's temperature profile. The error histogram reveals that the vast majority of prediction errors are concentrated very close to zero, with most falling within the ±0.02 range, which is negligible considering the temperature scale of approximately 350-500K. The function fit graph shows that the model accurately predicts the temperature curve shape, capturing both the initial rapid rise and the eventual plateau as the system approaches thermal equilibrium. These results validate the effectiveness of the ANN approach for modeling the thermal behavior of Case 2 PCM (Phase Change Material) configuration, providing a computationally efficient alternative to full CFD simulations for thermal system design and optimization.

8. Conclusion

The comprehensive analysis of thermal enhancement techniques for Phase Change Materials (PCMs) reveals significant insights into the performance of various configurations and the effectiveness of advanced modeling approaches. Through detailed examination of temperature evolution, velocity magnitude, and liquid fraction across multiple test cases, several key conclusions can be drawn.

1. The addition of nanoparticles consistently improves the thermal performance of PCMs across all tested configurations, as evidenced by faster heating rates and higher velocity magnitudes in the Nano PCM variants compared to their Pure PCM counterparts.
2. Case 2 and Case 3, which likely feature dendritic fins with downward-facing orientation, demonstrate superior thermal enhancement compared to other configurations. Their S-shaped liquid fraction curves indicate optimal melting progression through distinct phases of conduction-dominated initial heating, accelerated convection-dominated melting, and final slow completion.
3. The velocity magnitude data reveals complex flow dynamics within the PCM, particularly for Cases 2 and 3, where oscillatory behavior suggests beneficial periodic flow pattern changes that effectively distribute heat throughout the PCM volume.
4. The Artificial Neural Network (ANN) modeling approach has proven highly effective for predicting the thermal behavior of PCM systems, as demonstrated by the exceptional agreement between CFD simulation results and ANN predictions for both temperature profiles and liquid fraction curves in Case 2.

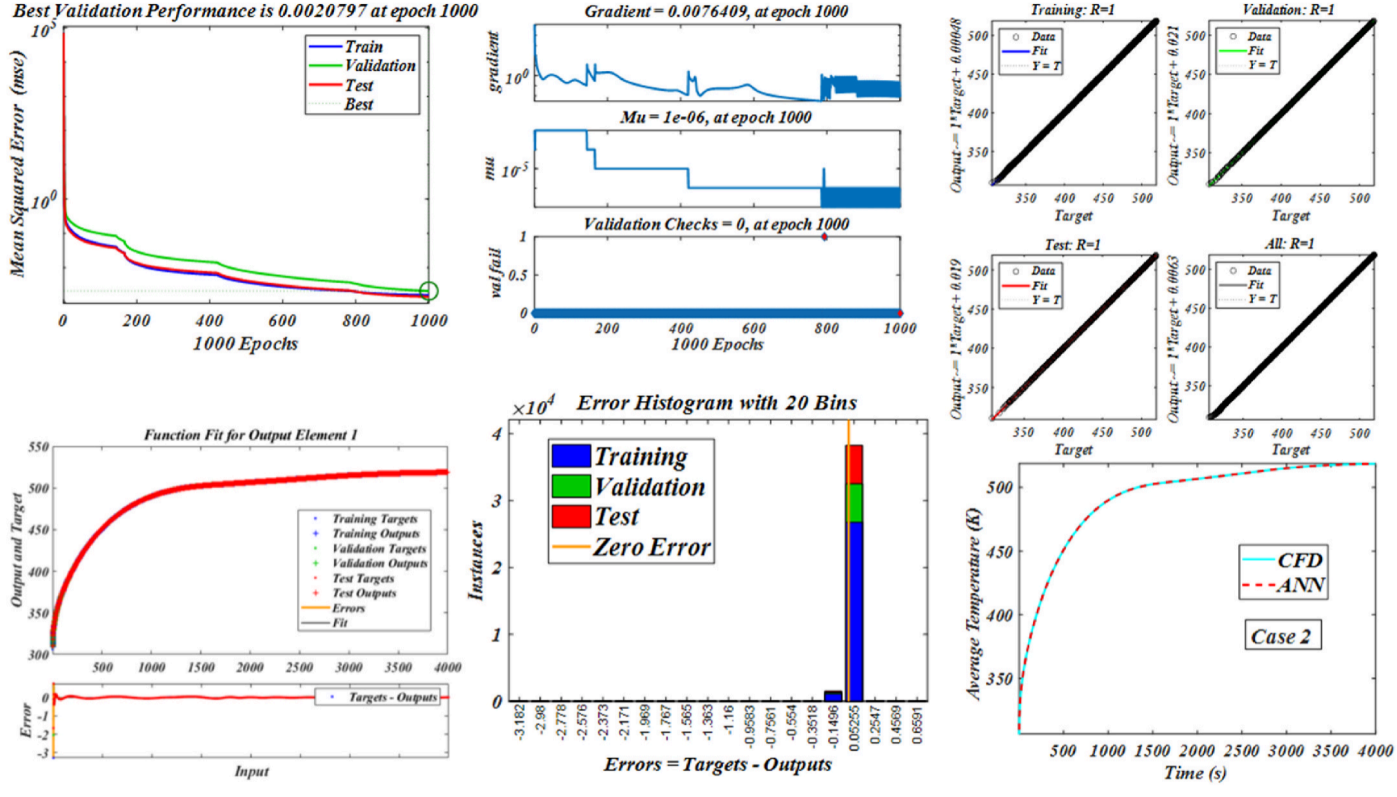

Figure 15. ANN performance for Case 2 (Temperature) showing excellent agreement with CFD results, with high regression accuracy (R = 1), low validation error (0.0020797), and minimal prediction error across datasets.

5. The training metrics, error histograms, and correlation analyses confirm the ANN model's reliability and accuracy, with R-values approaching 1 across all datasets and prediction errors concentrated very close to zero.
6. The combination of properly designed geometric features (likely dendritic fins with specific orientation) and nanoparticle addition represents a promising strategy for enhancing PCM thermal performance in various energy storage and thermal management applications.

This research contributes valuable insights to the field of thermal energy storage, offering both design guidelines for PCM system optimization and validation of efficient modeling approaches that can accelerate future thermal system development. The demonstrated ability to accurately predict complex phase-change thermal behavior using ANNs provides a computationally efficient alternative to resource-intensive CFD simulations, enabling more rapid design iteration and optimization.

CRediT authorship contribution statement

Hassan Waqas: Writing – review & editing, Supervision. **Meraj Ali Khan:** Resources, Formal analysis, Validation. **Mohib Hussain:** Writing – review & editing, Investigation. **Zunhua Zhang:** Writing – review & editing, Investigation, Formal analysis.

Declaration of competing interest

The authors declare no financial and non-financial interests.

Data availability

Data will be made available on request.

References

[1] M.N.A. Hawlader, M.S. Uddin, M.M. Khin, Microencapsulated PCM thermal-energy storage system, Appl. Energy 74 (2003) 195–202.
[2] W. Aftab, X. Huang, W. Wu, Z. Liang, A. Mahmood, R. Zou, Nanoconfined phase change materials for thermal energy applications, Energy Environ. Sci. 11 (2018) 1392–1424.
[3] E.M. Shchukina, M. Graham, Z. Zheng, D.G. Shchukin, Nanoencapsulation of phase change materials for advanced thermal energy storage systems, Chem. Soc. Rev. 47 (2018) 4156–4175.
[4] A.B. Colak, Numerical investigation of thermal energy storage in wavy enclosures with nanoencapsulated phase change materials using deep learning, Energy 320 (2025) 135272.
[5] N. Thirumalaivasan, S. Gopi, K. Karthik, S. Nangan, K. Kanagaraj, S. Rajendran, Nano-PCM materials: bridging the gap in energy storage under fluctuating environmental conditions, Process Saf. Environ. Prot. 189 (2024) 1003–1021.
[6] I. Benyahia, M.F. Al-Ghamdi, A. Abderrahmane, O. Younis, S. Laouedj, K. Guedri, A. Alahmer, Comprehensive thermal analysis of a nano-enhanced PCM in a finned latent heat storage system, Int. Commun. Heat Mass Tran. 165 (2025) 109106.
[7] M.X. Ho, C. Pan, Optimal concentration of alumina nanoparticles in molten Hitec salt to maximize its specific heat capacity, Int. J. Heat Mass Tran. 70 (2014) 174–184.
[8] M.G. Kibria, M.S. Mohtasim, U.K. Paul, B.K. Das, R. Saidur, Impact of hybrid nano PCM (paraffin wax with Al2O3 and ZnO nanoparticles) on photovoltaic thermal system: energy, exergy, exergoeconomic and enviroeconomic analysis, J. Clean. Prod. 436 (2024) 140577.
[9] M. Abdolahimoghadam, M. Rahimi, Experimental, numerical, and machine learning study of vertical thermal energy storage filling with novel hybrid nano- and bio-based phase change material, J. Energy Storage 106 (2025) 114815.
[10] M.M. Kenisarin, High-temperature phase change materials for thermal energy storage, Renew. Sustain. Energy Rev. 14 (2010) 955–970.
[11] B. Yu, W. Chen, Q. Liu, Z. Liao, C. Xu, Experimental analysis of the melting process of a high-temperature molten salt in a rectangular container, Energy 318 (2025) 134894.
[12] P. Yang, Y. Wang, Y. Yu, X. Wu, Numerical investigations on performance improvement of molten salt-based horizontal latent heat thermal energy storage unit with optimized structures, J. Energy Storage 98 (2024) 113203.
[13] S. Khalid, M. Hussain, H. Waqas, D. Liu, Enhancing thermal energy storage efficiency with nano-integrated phase change materials: machine learning-driven optimization via computational fluid dynamics, Int. Commun. Heat Mass Tran. 167 (2025) 109221.
[14] M. Lasfargues, A. Bell, Y. Ding, In situ production of titanium dioxide nanoparticles in molten salt phase for thermal energy storage and heat-transfer fluid applications, J. Nanoparticle Res. 18 (2016) 150.
[15] E.S. Hussain, I.Y. Hussain, Numerical study of performance enhancement of phase change material (PCM) thermal energy storage (TES) system by using nanoparticles, Al-Nahrain Journal for Engineering Sciences 28 (2025) 1–7.
[16] A. Andreozzi, P. Asinari, A. Barletta, V. Bianco, J.A. Bocanegra, P.V. Brandão, B. Buonomo, R. Cappabianca, M. Celli, E. Chiavazzo, Heat transfer and thermal energy storage enhancement by foams and nanoparticles, Energies 16 (2023) 7421.
[17] L. Kalapala, J.K. Devanuri, Influence of operational and design parameters on the performance of a PCM based heat exchanger for thermal energy storage–A review, J. Energy Storage 20 (2018) 497–519.
[18] J.M. Khodadadi, S.F. Hosseinizadeh, Nanoparticle-enhanced phase change materials (NEPCM) with great potential for improved thermal energy storage, Int. Commun. Heat Mass Tran. 34 (2007) 534–543.
[19] A.A. Ranjbar, S. Kashani, S.F. Hosseinizadeh, M. Ghanbarpour, Numerical heat transfer studies of a latent heat storage system containing nano-enhanced phase change material, Therm. Sci. 15 (2011) 169–181.
[20] N.S. Bondareva, M.A. Sheremet, Numerical simulation of heat transfer performance in an enclosure filled with a metal foam and nano-enhanced phase change material, Energy 296 (2024) 131123.
[21] Z. Rong, J. Ding, J. Lu, W. Wang, J. Yan, Experimental and theoretical investigation of an innovative composite nanofluid for solar energy photothermal conversion and storage, J. Energy Storage 52 (2022) 104800.
[22] A. Trigui, M. Abdelmouleh, Improving the heat transfer of phase change composites for thermal energy storage by adding copper: preparation and thermal properties, Sustainability 15 (2023) 1957.
[23] B. Muñoz-Sánchez, J. Nieto-Maestre, E. Veca, R. Liberatore, S. Sau, H. Navarro, Y. Ding, N. Navarrete, J.E. Julià, A.G. Fernández, Rheology of solar-salt based nanofluids for concentrated solar power. Influence of the salt purity, nanoparticle concentration, temperature and rheometer geometry, Sol. Energy Mater. Sol. Cell. 176 (2018) 357–373.
[24] C. Wu, Q. Wang, S. Sun, X. Wang, D. Cui, S. Pan, H. Sheng, Comprehensive thermal properties of ternary eutectic molten salt/nanoparticles composite phase change materials for high–temperature thermal energy storage, Sol. Energy Mater. Sol. Cell. 261 (2023) 112531.
[25] P.T. Sardari, H.I. Mohammed, D. Giddings, M. Gillott, D. Grant, Numerical study of a multiple-segment metal foam-PCM latent heat storage unit: effect of porosity, pore density and location of heat source, Energy 189 (2019) 116108.
[26] N. Ben Khedher, H. Togun, A.M. Abed, H.I. Mohammed, J.M. Mahdi, R.K. Ibrahem, W. Yaïci, P. Talebizadehsardari, A. Keshmiri, Comprehensive analysis of melting enhancement by circular Y-shaped fins in a vertical shell-and-tube heat storage system, Engineering Applications of Computational Fluid Mechanics 17 (2023) 2227682.
[27] P. Wang, H. Yao, Z. Lan, Z. Peng, Y. Huang, Y. Ding, Numerical investigation of PCM melting process in sleeve tube with internal fins, Energy Convers. Manag. 110 (2016) 428–435.
[28] N.A.A. Qasem, A. Abderrahmane, A. Belazreg, O. Younis, R.Z. Homod, M. Oreijah, K. Guedri, Influence of tree-shaped fins to enhance thermal storage units, Int. Commun. Heat Mass Tran. 151 (2024) 107220.
[29] C. Li, Z. Tang, H. Guo, Z. Li, M. Liang, Q. Li, Y. Wu, Investigation of melting performance enhancement in phase change material based shell and tube thermal energy storage device by using innovative hub-shaped longitudinal fins, J. Energy Storage 121 (2025) 116522.
[30] P.N.S. Teja, S.K. Gugulothu, G.R. Sastry, B. Burra, S.S. Bhurat, Numerical analysis of nanomaterial-based sustainable latent heat thermal energy storage system by improving thermal characteristics of phase change material, Environ. Sci. Pollut. Control Ser. 29 (2022) 50937–50950.
[31] T. Bouzennada, A. Abderrahmane, O. Younis, M. Oreijah, K. Guedri, C. Maatki, L. Kolsi, Numerical simulation of heat transfer and melting process in a NEPCM: using new fin shape, Int. Commun. Heat Mass Tran. 143 (2023) 106711.
[32] T. Bouzennada, F. Mechighel, A. Filali, L. Kolsi, Study of the usability of sinusoidal function heat flux based on enthalpy-porosity technique for PCM-Related applications, J. Therm. Anal. Calorim. 141 (2020) 1769–1784.
[33] J.M. Mahdi, E.C. Nsofor, Melting enhancement in triplex-tube latent thermal energy storage system using nanoparticles-fins combination, Int. J. Heat Mass Tran. 109 (2017) 417–427.
[34] X. Huang, S. Yao, X. Yang, R. Zhou, J. Luo, X. Shen, Comparison of solidification performance enhancement strategies for a triplex-tube thermal energy storage system, Appl. Therm. Eng. 204 (2022) 117997.